Effective Turn Fault Mitigation by Creating Zero Sequence Current Path for a Triple Redundant 3 × 3-Phase PMA SynRM

Bo Wang, *Member, IEEE*, Jiabin Wang, *Senior Member, IEEE*, Antonio Griffo, *Member, IEEE*, and Wei Hua, *Senior Member, IEEE*

***Abstract*—Effective mitigation of excessive stator turn fault current is crucial for fault tolerant machine drives. In this paper, a simple and effective method is proposed for a triple redundant 3 × 3-phase permanent magnet-assisted synchronous reluctance machine by using three 3-phase 4-leg inverters. The fourth leg creates a zero sequence current path when a terminal short circuit is applied in an event of a turn fault in a 3-phase winding set. Consequently, the zero sequence flux linkages are reduced by the resultant zero sequence current. This leads to lower residual flux linkage and decreased fault current. The machine drive can therefore have larger safety margin or can be designed for improved torque density and efficiency. The proposed approach is verified by both finite element (FE) simulations and experimental tests in a wide operation range. It shows that the fault current is reduced by ∼40% and the output torque is not affected.**

***Index Terms*—3-phase 4-leg inverter, fault location, fault tolerant, flux nullifying, terminal short circuit, turn fault, zero sequence current.**

I. Introduction

ELECTRICAL machine drives are being increasingly used in various applications due to the merits of high torque/power density, high efficiency, improved control performance, and flexibility in configuration and deployment [1]. During operation, the stator winding is exposed to the electrical loading, thermal cycling, aging, vibration, and environmental contamination. As a result, the insulation material degrades gradually and finally loses its insulating characteristics [2]. Consequently, various electric faults may occur in the machine drives, such as open circuit, short circuit, and turn fault [3], [4]. Among these faults, turn fault, also commonly referred to as inter-turn short-circuit fault, is known to be the worst fault case since a turn fault that involves a few turns in the short circuited path will result in extremely large fault current and causes

Manuscript received September 27, 2018; revised December 19, 2018 and January 28, 2019; accepted February 13, 2019. Date of publication February 20, 2019; date of current version August 29, 2019. Recommended for publication by Associate Editor B. Singh. *(Corresponding author: Bo Wang.)*

B. Wang and W. Hua are with the School of Electrical Engineering, Southeast University, Nanjing 210096, China (e-mail:

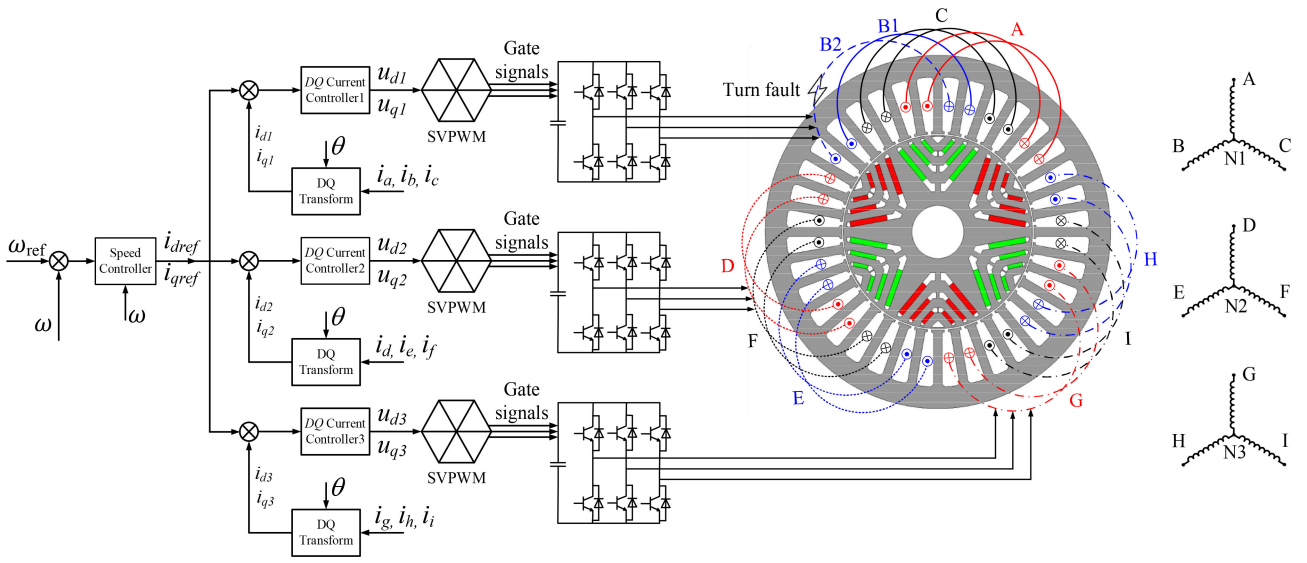

Fig. 1. PMA SynRM with segregated windings and independent drives.

In order to avoid the damage effect of excessive turn fault current, a novel mitigation method is proposed for a triple redundant 3 × 3-phase permanent magnet-assisted synchronous reluctance machine (PMA SynRM) drive using 3-phase 4-leg inverters. The fourth leg provides a zero sequence current path in the faulted 3-phase set; as a result, the zero sequence short circuit currents can flow and zero sequence flux linkage is essentially nullified. As a result, the residual flux linkage of the fault turns is further reduced, resulting in lower fault current. The approach is explained in detail and the effect of the zero sequence current is analyzed in subsequent sections. The effectiveness of the proposed method is validated by extensive finite element (FE) simulation and experimental tests in a wide operation range.

II. Turn Fault Behavior of the Triple Redundant 3 × 3-Phase PMA SynRM

The machine under consideration is a triple redundant 3 × 3-phase PMA SynRM aiming for an aerospace application requiring high availability as shown in Fig. 1. PMA SynRM explores both PM torque and reluctance torque. The PM torque contributes only a small proportion of the total torque. The reluctance torque enables less use of magnets without decreasing the torque capability, therefore, exhibiting comparable performance with conventional surface mounted PM machines (SPM). The low PM field reduces the fault current in case of a short-circuit fault. It also eliminates the possibility of uncontrolled generation at high speed. Unlike the SPM, the torque purely relies on the PM field and, consequently, the increase in torque capability leads to higher flux linkage. The presence of strong PM field poses a safety hazard to the machine as it cannot be turned off in the event of a fault. Therefore, PMA SynRM with less magnets is favored in fault tolerant application.

The PMA SynRM specifications are given in Table I [15], [16]. The conventional overlapped windings of the PMA SynRM have been divided into three sets of separated 3-phase windings with each set being not overlapping with the others. Each 3-phase set is star-connected and driven by an independent standard 3-phase inverter using *dq* current controller. The three neutrals are not connected to ensure electrical isolation. Otherwise, the three 3-phase winding sets will affect each other in faulty operation conditions. As a result, the different 3-phase sets are physically, thermally, and electrically isolated. In case of a fault in one 3-phase set either in the windings or in the specific inverter, it can be mitigated by deactivating the fault set inverter or applying TSC on the fault windings while the remaining two 3-phase winding sets can still operate to produce about two-thirds torque. In fault operation, the *dq* current controller tracks the current commands for each 3-phase winding automatically by adjusting the voltage vectors.

TABLE I
Specifications of the Machine

Specification	Symbol	Value
Base speed	n_b	4 000 rpm
Maximum speed	n_m	19 200 rpm
Rated power	P_r	33.5 kW
Rated current and gamma angle	I_{rated}	120 A (51°)
Nominal DC link voltage	V_{dc}	270 V
Turn number of each coil	N	8
Faulty turn number	N_f	1

It should be noted though the machine winding is designed to be physically, thermally, and electrically isolated, it is not magnetically isolated. The currents of one 3-phase set can affect the operation of the other two sets via magneto-motive force (MMF) distribution. Hence, a fault in one 3-phase set is also influenced by the other two sets. In terms of the worst fault case, inter-turn short circuit, the excessive fault current can be alleviated by applying TSC on the fault 3-phase set. After TSC, the resultant short-circuit phase currents tend to reduce the flux linkage in the fault turns and consequently, the fault current decreases. However, it was shown that the fault current after the application of TSC is dependent on the fault coil location, namely, A1, A2, . . . , C1, C2. According to the investigation in

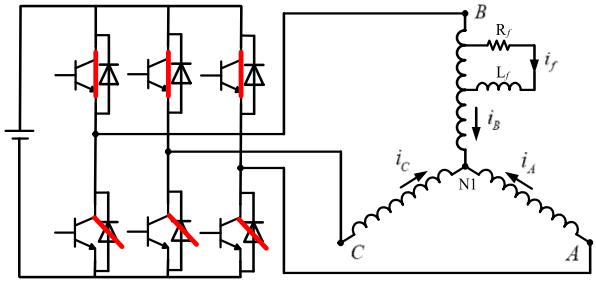

Fig. 2. Illustration of TSC after turn fault.

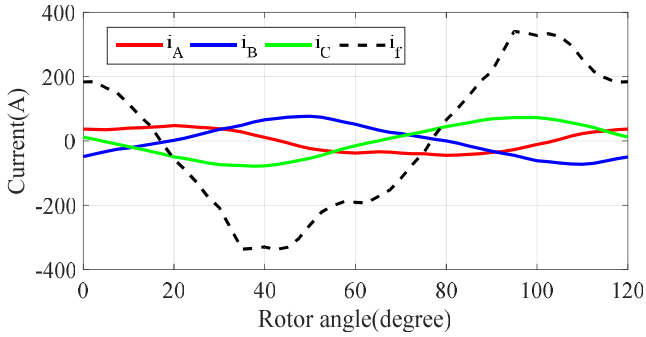

Fig. 3. Simulated turn fault current and phase currents of set ABC with turn fault in coil B2 after TSC.

[15], [17], the fault current is the highest if the fault occurs in coil B2 in motoring mode, which is the trailing coil of set ABC (assuming that the machine is rotating anti-clockwise). On the contrary, it is the highest in coil A1 in generating mode that corresponds to the leading coil.

By way of example, a single turn fault in coil B2 after TSC is simulated in Cedrat Flux while the other two healthy 3-phase sets are excited with 120A-rated currents with 51° gamma angle at 4000 r/m in motoring mode. This angle is between the q-axis and the current vector corresponding to the maximum torque per ampere operation. Since the remaining windings still operate in balanced manner, the maximum torque per Ampere (MTPA) curves of the healthy and faulty operation are very close. So the machine still follows the healthy MTPA curve in post fault operation. As shown in Fig. 2, the faulted set ABC can be short circuited by turning on all the top or bottom switches of the inverter. The turn fault is emulated by short circuiting one turn winding with zero external impedance. Meanwhile, ideal current sources are used to represent the inverter drives for two remaining healthy 3-phase sets DEF and GHI under closed-loop current control. The simulated turn fault current and phase currents are shown in Fig. 3.

It is seen that the resultant phase currents are unbalanced and contain mainly the positive and negative sequence components [18]. It is evident that the turn fault current is still higher than the rated value (∼2.6 per unit (p.u.) with respect to the rms rated current). This high fault current implies that the flux linkage of the fault turns is not effectively nullified. It is worth noting that the machine in Table I is thermally designed to cope with the worst case turn fault current in coil B2 in motoring mode with rated current excitation. The temperature of the fault turn should

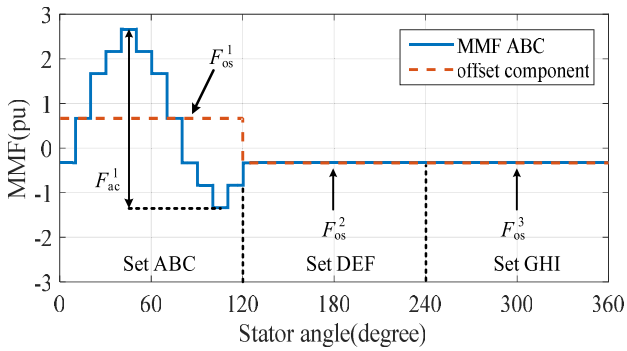

Fig. 4. MMF produced by set ABC.

be lower than the maximum allowable temperature of the copper wires. Due to the excessive fault current, the machine has to be designed with less magnets. Hence, the efficiency and the torque capability of the machine are compromised. However, if this fault current is further reduced, the machine can be optimized for improved torque density and efficiency. Thus, it would be desirable if the turn fault current could be further reduced.

III. Analysis of the Conventional Turn Fault Mitigation Method TSC

In order to develop an effective method to reduce the turn fault current, the effect of the conventional mitigation action TSC on the turn fault is analyzed. After the application of TSC on the fault set, which can be conveniently implemented by setting the inverter reference voltages to zero, the phase currents of the fault 3-phase set are governed by (1) where i_{d1}, i_{q1} and ψ_{d1}, ψ_{q1} are the dq-axis currents and flux linkages of the ABC set, respectively. R is the phase resistance and ω is the electrical angular speed,

$$0 = Ri_{d1} + \frac{d\psi_{d1}}{dt} - \omega\psi_{q1}\,, 0 = Ri_{q1} + \frac{d\psi_{q1}}{dt} + \omega\psi_{d1}. \quad (1)$$

After the application of TSC, ψ_{d1}, ψ_{q1} contain significant second harmonics since the symmetry is broken. And hence, the induced short-circuit currents of the fault set become unbalanced. Meanwhile, the two remaining healthy sets are still excited by load currents with closed-loop current controller. Significant negative and zero sequence flux linkage components arise in the fault set due to unbalanced operation. It can be described by the resultant MMF, which is calculated by multiplying the winding functions of the machine with their phase currents [19], [20]. According to the work presented in [21], a typical MMF induced by the currents in set ABC only is shown in Fig. 4. It is seen that the currents in set ABC produce MMF not only over the set itself but also over the other two sets. More specifically, the MMF over set ABC consists of an AC component $F_{\rm ac}^1$, and an offset component $F_{\rm os}^1$ while only an offset component $(F_{\rm os}^2,\ F_{\rm os}^3)$ exists over other regions. In fact, the different 3-phase set affects the other sets via the MMF offset component.

The total MMF over the whole air gap equals the summation of MMF induced by the three sets. It can be divided into three parts, each being associated with the region occupied by one 3-phase winding. The typical MMF over one 3-phase set

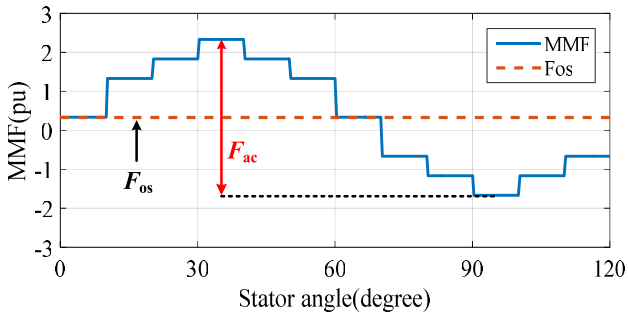

Fig. 5. MMF over set ABC region.

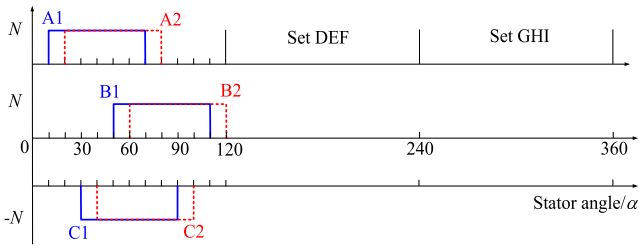

Fig. 6. Turn functions of the coils in set ABC.

region, F, is illustrated in Fig. 5 for set ABC. It consists of an AC component $F_{\rm ac}$, and an offset component $F_{\rm os}$. The AC component $F_{\rm ac}$ is purely determined by the currents in that set while the offset component $F_{\rm os}$ is the combined effect of the currents in all three 3-phase sets.

The flux density of the armature reaction in the air gap and the resultant flux linkage are proportional to the MMF distribution. The MMF AC component $F_{\rm ac}$ is the same as that of healthy condition and the induced flux linkage also has a sinusoidal distribution if the high-order harmonics are ignored. However, the flux linkage produced by the MMF offset component $F_{\rm os}$ has a different characteristic.

Taking phase A as an example, the flux linkage $\varphi_{\rm osA}$ produced by the offset component $F_{\rm os}$ can be evaluated by (2) where $\varphi_{\rm osA1}$ and $\varphi_{\rm osA2}$ denote the resultant flux linkages for coils A1 and A2, respectively. $n_{\rm A1}$, $n_{\rm A2}$ are the turn functions for coils A1 and A2 as shown in Fig. 6. r is the radius of the stator inner bore and l is the axial length of the stator stack. $g^{-1}(\alpha)$ is the inverse air gap function given in (3). The resultant flux linkages in phases B and C, $\varphi_{\rm osB}$ and $\varphi_{\rm osC}$, can be derived similarly as

$$\begin{aligned}\varphi_{\rm osA} &= \varphi_{\rm osA1} + \varphi_{\rm osA2} \\ &= \mu_0 r l \int g^{-1}(\alpha)\left(n_{\rm A1}+n_{\rm A2}\right) F_{\rm os} d\alpha \qquad (2)\end{aligned}$$

$$g^{-1}(\alpha) = a + b\cos\left(2\alpha+\alpha_0\right). \qquad (3)$$

Since the coils are full-pitched and the MMF offset component $F_{\rm os}$ is constant over the ABC set region, it can be inferred that $\varphi_{\rm osA1}$ equals $\varphi_{\rm osA2}$ and is half of $\varphi_{\rm osA}$. Further, it can be deduced that $\varphi_{\rm osA}$ equals $\varphi_{\rm osB}$. Due to the opposite polarity of the turn function for phase C compared to that of phases A and B, the offset flux linkage of phase C has the same magnitude but an opposite polarity as given in (4) and shown in Fig. 7

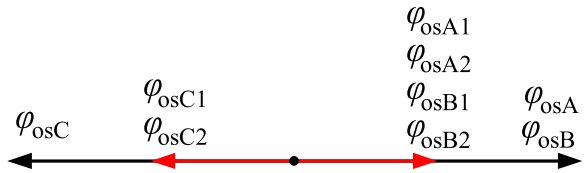

Fig. 7. Relationship of the phase and coil flux linkages due to the MMF offset component.

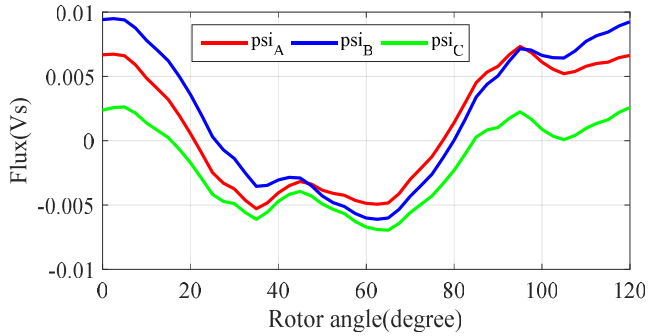

Fig. 8. Phase flux linkages of set ABC after TSC when two remaining healthy 3-phase sets are excited with rated currents in motoring mode.

$$\varphi_{\rm osA} = \varphi_{\rm osB} = -\varphi_{\rm osC}. \qquad (4)$$

The above-mentioned flux linkages vary with the MMF offset component $F_{\rm os}$. It is evident from (4) that the flux linkage produced by the MMF offset component not only contains positive and negative sequence components but also has zero sequence component φ_0 as given in (5) as follows:

$$\varphi_0 = \left(\varphi_{\rm osA}+\varphi_{\rm osB}+\varphi_{\rm osC}\right)/3 = \varphi_{\rm osA}/3. \qquad (5)$$

For the star-connected 3-phase winding, positive and negative sequence currents can be generated by the application of TSC in the fault 3-phase set to counteract the corresponding flux linkages of the faulted turns. As a result, the positive and negative sequence flux linkage components are reduced to a much lower value. However, the zero sequence flux linkage remains since there is no path for the zero sequence current. Hence, it can be concluded that the zero sequence flux linkage of the fault turns is the main cause of the high fault current seen in Fig. 3.

The typical phase flux linkages of set ABC after TSC when the other two healthy sets are excited by 120 A currents in motoring mode are simulated in FE and plotted in Fig. 8. As can be seen, the residual flux linkages have similar waveforms and phase shifts. Obviously, majority of the flux linkages are zero sequence components because there is no zero sequence current in the star-connected winding. As a result, in the event of a turn fault, the residual flux linkage of the fault turns after TSC is mainly due to the zero sequence flux linkage.

The flux linkage of each phase equals the summation of the two subcoils. Thus, the flux linkages of the six coils are further shown in Fig. 9. It is seen that the flux linkages of the six coils

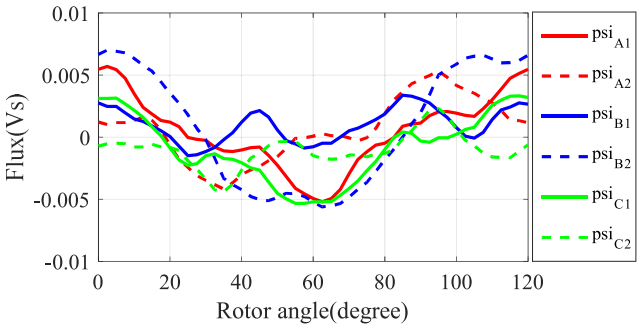

Fig. 9. Flux linkages of the six coils in set ABC after TSC when two remaining healthy sets are excited with rated currents in motoring mode.

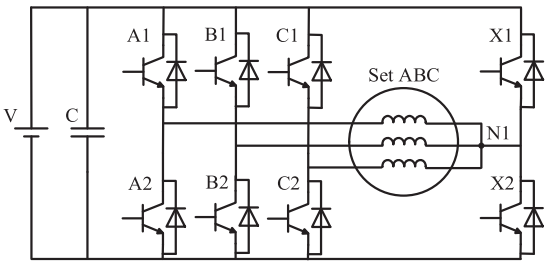

Fig. 10. 3-phase 4-leg inverter for set ABC.

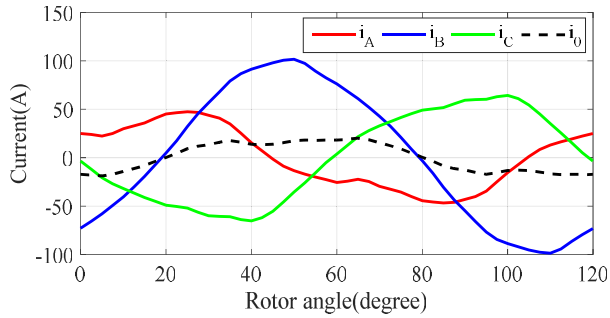

Fig. 11. Phase currents and zero sequence current of set ABC after TSC with zero sequence current path.

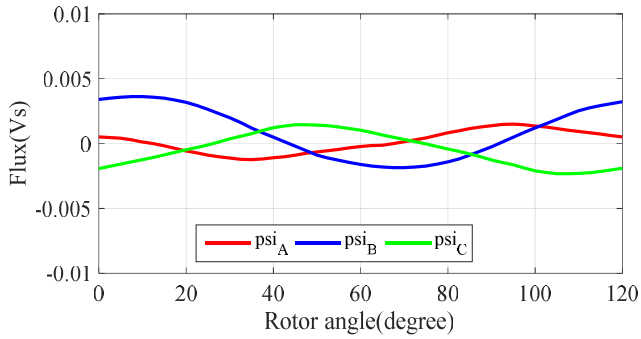

Fig. 12. Phase flux linkages of set ABC after TSC with zero sequence current path.

are quite different from each other. This explains why the fault current is different if the turn fault occurs in different coils. Since the residual flux linkage of coil B2 is the highest, the fault current will be the highest if the turn fault occurs in coil B2. This finding is consistent with the conclusion drawn in [15]. The machine fault behavior in generating mode is similar and therefore the analysis is not repeated. The only difference is that the residual flux linkage of coil A1 will be the highest, which will lead to the highest turn fault current if the turn fault occurs in coil A1.

IV. Proposed Mitigation Method by Creating Zero Sequence Current Path

According to the aforementioned analysis, the excessive turn fault current after TSC is mainly due to the zero sequence flux linkage. If a zero sequence current path can be created for the 3-phase winding, zero sequence short-circuit currents will be induced in the windings. Consequently, the zero sequence flux linkages in the fault turns will be lower and the fault current will be reduced accordingly.

A zero sequence current path can be provided by using 3-phase 4-leg inverter [22], [23]. The neutral point of the 3-phase winding is connected to the fourth leg as shown in Fig. 10 for set ABC to provide a zero sequence current path. The same inverter topology is used to drive sets DEF and GHI. In healthy condition, the machine is fed by the three 3-phase inverters with the fourth leg inactive. So, the machine performance has no difference with the standard full bridges. However, in case of a turn fault, all the four top or bottom switches of the 3-phase 4-leg inverter can be closed to apply TSC on the fault set. With the aid of the fourth leg, a zero sequence current path is created. And hence zero sequence currents can flow in the windings via the neutral path and nullify the zero sequence flux linkages. Consequently, the residual fault linkage of the fault turns is further reduced, implying lower fault current. Meanwhile, the other two healthy winding sets operate as normal to provide output torque.

In order to illustrate the effect of the zero sequence current on the zero sequence flux linkages, TSC is applied to set ABC without turn fault by switching ON all the four top switches of the 3-phase 4-leg inverter when the other two healthy sets are excited by 120 A currents in motoring mode. The resultant phase currents and zero sequence current are shown in Fig. 11. The phase currents are also unbalanced and the induced zero sequence current is less than 20 A. The resultant residual phase flux linkages of set ABC are plotted in Fig. 12. As can be seen, the magnitudes of the flux linkages are much lower than those without zero sequence current path shown in Fig. 8. The original zero sequence flux linkages are effectively nullified by the induced zero sequence currents. And hence, the residual flux linkages in Fig. 12 are quite different with those of Fig. 8.

In addition, the flux linkages of the six coils in set ABC are shown in Fig. 13. The flux linkage of coil B2 is still the highest while its amplitude is reduced by 40% compared with that in Fig. 9. It can be seen that the residual flux linkages are significantly reduced due to the zero sequence current. As a result, the turn fault current would be lower accordingly.

The machine behavior with single turn fault in coil B2 after TSC with the proposed zero sequence current path is simulated

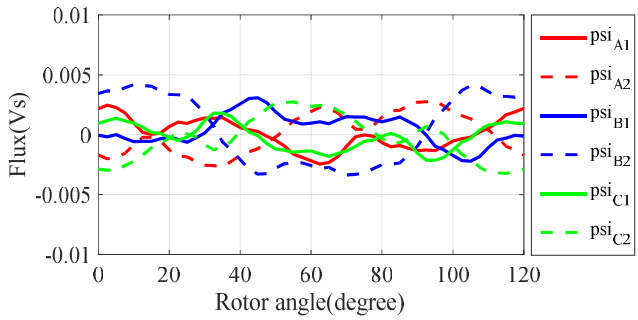

Fig. 13. Flux linkages of the six coils in set ABC after TSC with zero sequence current path.

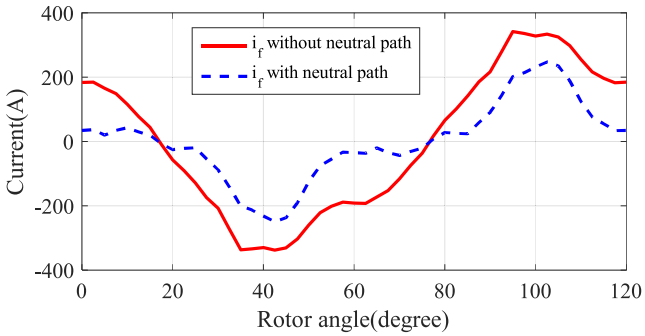

Fig. 14. Comparison of the turn fault current in coil B2 after TSC with and without zero sequence current path.

in FE while the other two healthy sets are still loaded by the rated currents at 4000 r/m in motoring mode. The resultant turn fault current is plotted in Fig. 14 and compared with the fault current without neutral path. It is seen that the rms fault current has been reduced from 220 A (2.6 p.u.) to 121A (1.42 p.u.). It results in 70% reduction in the copper loss of the fault turn. And since the 1.42 p.u. fault current flows only in the fault turn while the currents in the remaining windings are lower than the rated value, the heat of fault current can be effectively dissipated and the temperature rise in the fault turn in quite mild.

Similarly, the concept is also validated for the worst case in generating mode with single turn fault in coil A1. TSC is applied on the fault set while the other two healthy sets are loaded with the rated currents at 4000 r/m. The resultant turn fault currents with and without the zero sequence current path are compared in Fig. 15. As can be seen, the rms value has also been reduced from 230 A (2.7 p.u.) to 158 A (1.9 p.u.).

Due to the decreased fault current, the copper loss of the fault turn is significantly reduced and leads to lower temperature rise. As a result, the machine could have larger safe margin under this severe fault. On the other hand, the constraint to accommodate the fault current is eased and the machine can be optimized for better torque density and efficiency. It should be noted that the fourth leg will introduce additional cost to the drive system. However, the current in the fourth leg is quite small due to the low zero sequence current. Therefore, it can be designed with a small current rating by low-cost switch devices. Hence, the additional cost is quite minor compared to the whole machine drive. In addition, by using the zero sequence current,

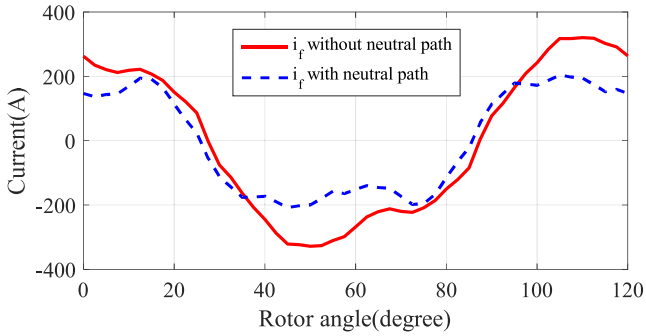

Fig. 15. Comparison of the turn fault current in coil A1 after TSC with and without zero sequence current path.

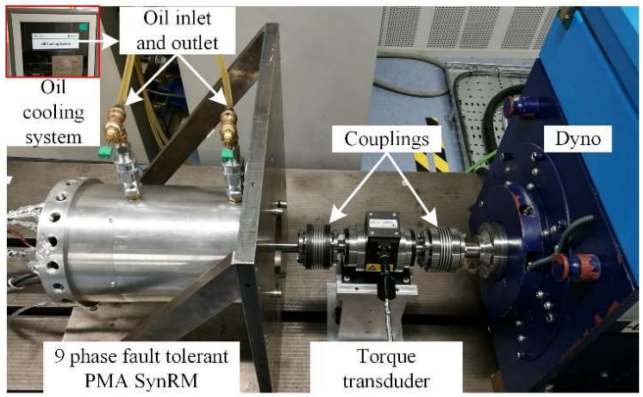

Fig. 16. 9-phase PMA SynRM test rig.

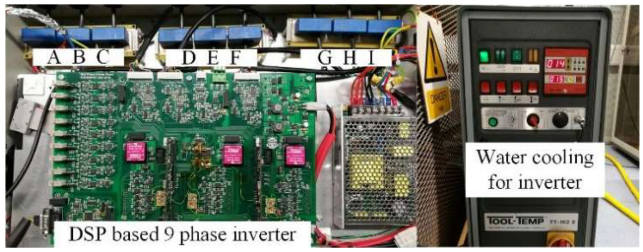

Fig. 17. DSP-based 9-phase inverter.

the machine drive could gain increased torque capability in an event of 1-phase open circuit fault as described [22], [23].

V. Experimental Validation

The proposed turn fault mitigation method has been tested on a triple redundant 3 × 3-phase PMA SynRM prototype whose specifications are given in Table I. The machine is mounted on the dynamometer via the torque transducer as shown in Fig. 16. During the tests, the dyno is controlled at a given speed rotating with the machine prototype. The machine is driven by an existing digital signal processor (DSP)-controlled 9-phase inverter, consisting of three 3-phase standard inverters as shown in Fig. 17. It is controlled by classic *dq* current controller. After the turn fault, the voltage vectors are adjusted automatically by the *dq* current controller to track the current commands while the fault set is protected by TSC. The inverter switches are

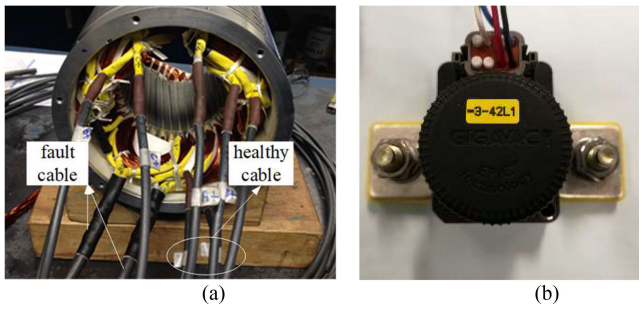

Fig. 18. Turn fault test setup. (a) Cable leads. (b) Relay.

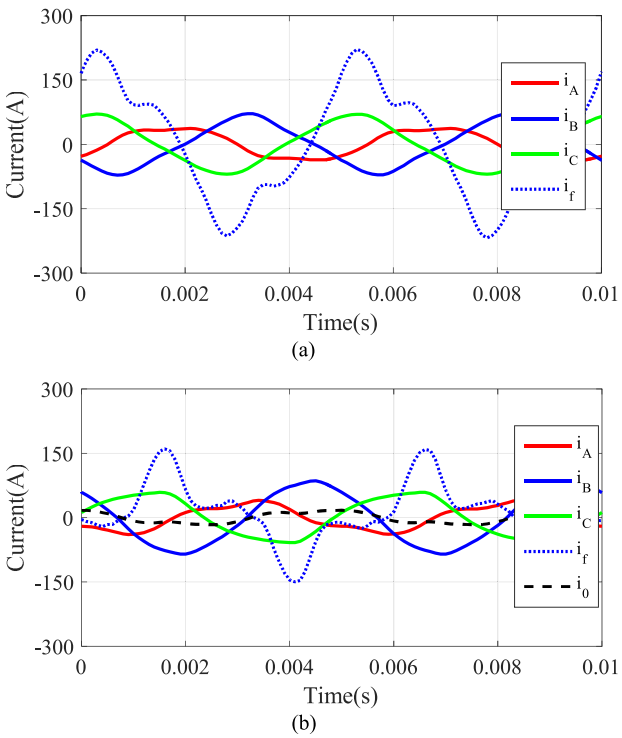

Fig. 19. Turn fault current and phase currents with turn fault in coil B2 in motoring mode at 4000 r/m after TSC. (a) Without neutral path. (b) With neutral path.

modulated by SVPWM at 10 kHz. The zero sequence current path in turn fault condition is realized by short circuiting the neutral and the 3-phase terminals directly.

The experimental setup for the turn fault emulation is illustrated in Fig. 18. A single turn tap is brought out in coil B2 of set ABC. Two thick cables are soldered to the fault turn taps to minimize the additional impedance in the short-circuit path. The leads are connected to a relay for controlled fault emulation. The turn fault can be sensed by monitoring the second harmonic in the instantaneous active power in generating mode or the second harmonic in the reactive power in motoring mode according to the work presented in [24].

A. Turn Fault in Coil B2

First, the machine is tested with a single turn fault in coil B2 at the base speed of 4000 r/m. TSC has been applied on the fault ABC set for both without and with zero sequence current

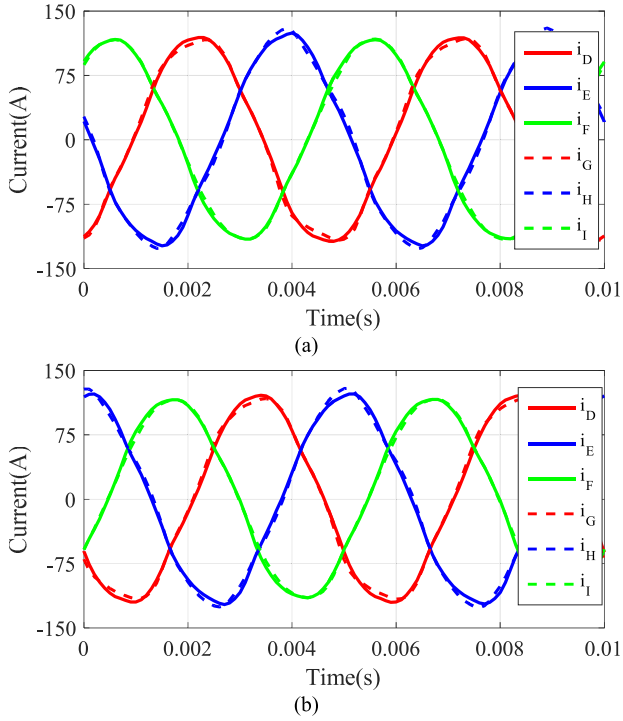

Fig. 20. Healthy phase currents with turn fault in coil B2 in motoring mode at 4000 r/m after TSC. (a) Without neutral path. (b) With neutral path.

path. Meanwhile, the other two healthy sets are excited with 120 A currents. The resultant fault current and phase currents in set ABC are compared in Fig. 19. As can be seen, the rms turn fault current has been reduced from 130 to 76 A due to the zero sequence current path. The amplitude of the induced zero sequence current is 17 A. Fig. 20 compares the phase currents in the healthy sets where negligible difference is seen. The small zero sequence current in set ABC has insignificant impact on the operation of the two healthy sets.

Compared with Fig. 14, the measured turn fault currents are lower than the simulated results. It can be attributed to the additional impedance caused by the lead cable and relay in experimental test. The estimated resistance and inductance due to the lead cable and relay are 1.5 mΩ and 1 μH, respectively. When the external impedance is considered in FE simulation under the same operation conditions, the simulated and tested turn fault currents coincide very well for both without neutral path and with path scenarios as shown in Fig. 21, confirming the effectiveness of the proposed method.

It should be noted that due to the limited number of current probes of the oscilloscope, the 9-phase currents and fault current are mainly measured by the inverter current sensors, and consequently the switching harmonics are not visible in the current waveforms due to limited sampling frequency and anti-alias filtering.

In addition, the output torque variations with load current in the two healthy set are compared in Fig. 22 for the two fault mitigation schemes, namely, TSC on set ABC with and without zero sequence current path. It is seen that the zero sequence current also has negligible influence on the output torque. The

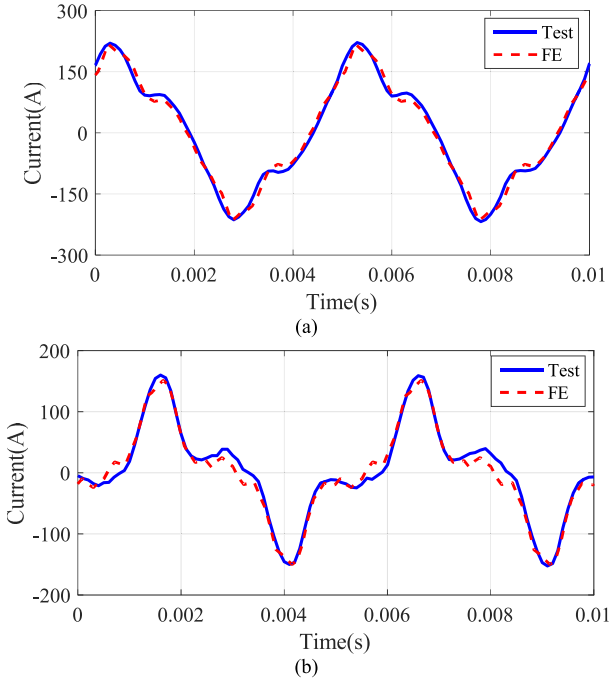

Fig. 21. Turn fault current comparisons in coil B2 in motoring mode at 4000 r/m after TSC. (a) Without neutral path. (b) With neutral path.

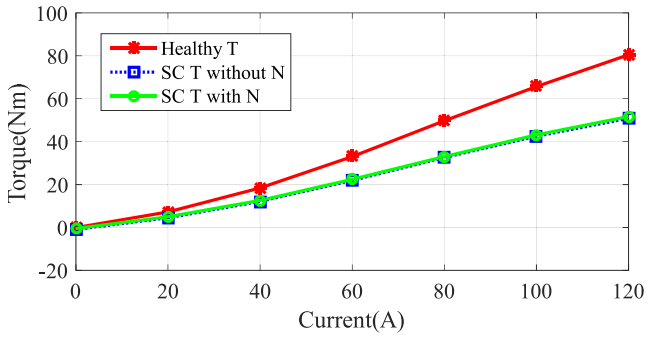

Fig. 22. Comparison of the output torques.

machine is still capable to output about two-thirds of the torque in healthy condition. The rms turn fault current variations with the load current under the two different scenarios are compared in Fig. 23 for both motoring and generating modes. It is evident that the turn fault current is reduced and well limited within 1 p.u. in all operation conditions. Therefore, the turn fault current will not cause any thermal issue after introducing the zero sequence current path.

B. Turn Fault in Coil A1

The machine is also tested with single turn fault in coil A1 by reverse rotation of the rotor. Consequently, the turn fault in coil B2 (trailing coil for anti-clockwise rotation) becomes equivalent to the leading coil A1 in clockwise rotation. TSC without and with zero sequence current path is also applied on set ABC while the two healthy sets are still loaded by 120 A at 4000 r/m in generating mode. The resultant phase currents are similar and therefore, only the turn fault currents are shown

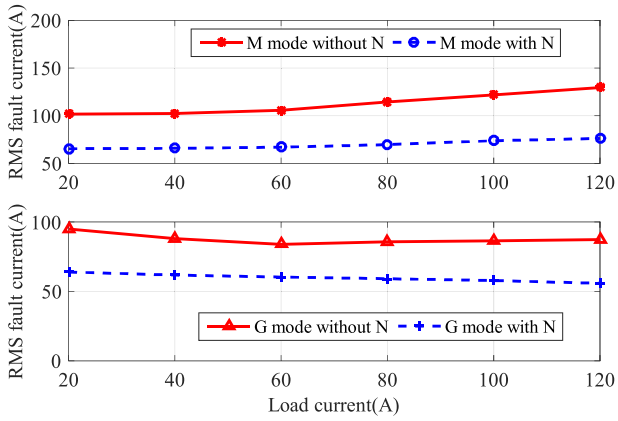

Fig. 23. Comparison of the turn fault current variations with the load current in coil B2.

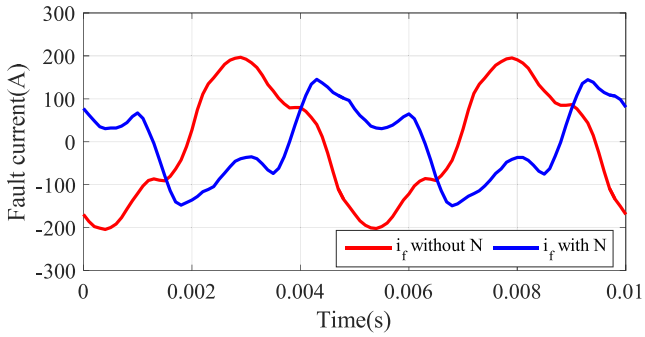

Fig. 24. Comparison of the turn fault current with turn fault in coil A1.

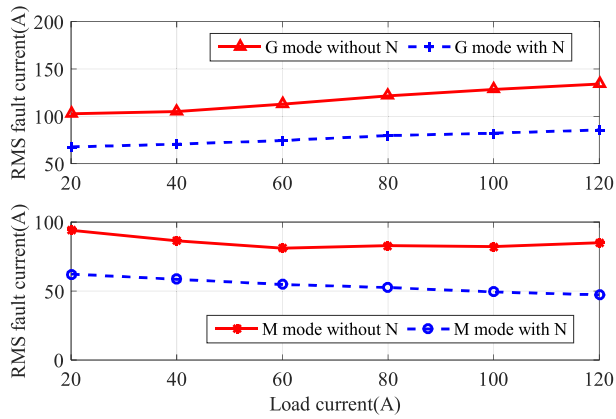

Fig. 25. Comparison of the turn fault current variations with the load current in coil A1.

in Fig. 24. It is seen that the rms fault current is also reduced from 134 to 85 A due to the zero sequence current path via the neutral connection. It should be noted that the two waveforms are measured separately; however, they are plotted on the same time axis. Similarly, the rms turn fault current variation with the load current under the two different scenarios is compared in Fig. 25 for both motoring and generating modes. The reduction of the turn fault current with the neutral path is also seen in all operation conditions.

VI. Conclusion

In this paper, a simple and effective method for turn fault mitigation has been developed for a triple redundant 3 × 3-phase PMA SynRM by using 3-phase 4-leg inverters. The fourth leg can be used to create zero sequence current path after the application of TSC. Therefore, the zero sequence flux linkages are further reduced by the induced zero sequence current. Both the flux linkage of the fault turns and the fault current are reduced effectively. The approach has been extensively verified by both FE simulations and experimental tests. It has been shown that the fault current is reduced by ∼40% in all operation ranges and the output torque is not compromised. The proposed mitigation method offers larger safety margin and allows the machine to be optimized for improved torque capability and efficiency. The additional cost due to the fourth leg may be justified for improved fault tolerance and higher output torque in open-circuit fault. The proposed fault mitigation concept to reduce turn fault current is applicable to other multi-phase machines.

References

[1] J. Wang, Z. P. Xia, and D. Howe, "Three-phase modular permanent magnet brushless machine for torque boosting on a downsized ICE vehicle," *IEEE Trans. Veh. Technol.*, vol. 54, no. 3, pp. 809–816, May 2005.

[2] B. G. Gu, J. H. Choi, and I. S. Jung, "Development and analysis of interturn short fault model of PMSMs with series and parallel winding connections," *IEEE Trans. Power Electron.*, vol. 29, no. 4, pp. 2016–2026, Apr. 2014.

[3] H. Zhou, W. Zhao, G. Liu, R. Cheng, and Y. Xie, "Remedial field-oriented control of five-phase fault-tolerant permanent-magnet motor by using reduced-order transformation matrices," *IEEE Trans. Ind. Electron.*, vol. 64, no. 1, pp. 169–178, Jan. 2017.

[4] L. Parsa and H. A. Toliyat, "Fault-tolerant interior-permanent-magnet machines for hybrid electric vehicle applications," *IEEE Trans. Veh. Technol.*, vol. 56, no. 4, pp. 1546–1552, Jul. 2007.

[5] D. C. Patel and M. C. Chandorkar, "Modeling and analysis of stator interturn fault location effects on induction machines," *IEEE Trans. Ind. Electron.*, vol. 61, no. 9, pp. 4552–4564, Sep. 2014.

[6] J. K. Park and J. Hur, "Detection of inter-turn and dynamic eccentricity faults using stator current frequency pattern in IPM-type BLDC motors," *IEEE Trans. Ind. Electron.*, vol. 63, no. 3, pp. 1771–1780, Mar. 2016.

[7] P. Arumugam, C. Gerada, T. Hamiti, C. Hill, and S. Bozhko, "A review on turn-turn short circuit fault management," in *Proc. Int. Conf. Electr. Syst. Aircr., Railway, Ship Propulsion Road Veh.*, 2015, pp. 1–5.

[8] B. C. Mecrow, A. G. Jack, J. A. Haylock, and J. Coles, "Fault-tolerant permanent magnet machine drives," *IEE Proc.—Elect. Power Appl.*, vol. 143, no. 6, pp. 437–442, Nov. 1996.

[9] J. G. Cintron-Rivera, S. N. Foste, and E. G. Strangas, "Mitigation of turn-to-turn faults in fault tolerant permanent magnet synchronous motors," *IEEE Trans. Energy Convers.*, vol. 30, no. 2, pp. 465–475, Jun. 2015.

[10] A. J. Mitcham, G. Antonopoulos, and J. J. A. Cullen, "Implications of shorted turn faults in bar wound PM machines," *IEE Proc. Elect. Power Appl.*, vol. 151, no. 6, pp. 651–657, Nov. 2004.

[11] J. Chai, J. Wang, K. Atallah, and D. Howe, "Performance comparison and winding fault detection of duplex 2-Phase and 3-Phase fault-tolerant permanent magnet brushless machines," in *Proc. Ind. Appl. Annu. Meeting*, 2007, pp. 566–572.

[12] P. F. Turnbull, S. L. Hayslett, H. J. Bauer, D. J. Berry, and G. D. Dolan, "Method and apparatus for controlling an electric machine," U.S. 9 242 576 B1, Jan. 2016.

[13] X. Tu, L. A. Dessaint, M. E. Kahel, and A. O. Barry, "A new model of synchronous machine internal faults based on winding distribution," *IEEE Trans. Ind. Electron.*, vol. 53, no. 6, pp. 1818–1828, Dec. 2006.

[14] X. Tu, L. A. Dessaint, N. Fallati, and B. D. Kelper, "Modeling and real-time simulation of internal faults in synchronous generators with parallel-connected windings," *IEEE Trans. Ind. Electron.*, vol. 54, no. 3, pp. 1400–1409, Jun. 2007.

[15] B. Wang, J. Wang, and A. Griffo, "A fault tolerant machine drive based on permanent magnet assisted synchronous reluctance machine," in *Proc. IEEE Energy Convers. Congr. Expo.*, Milwaukee, WI, USA, 2016, pp. 1–8.

[16] B. Wang, J. Wang, B. Sen, A. Griffo, Z. Sun, and E. Chong, "A fault tolerant machine drive based on permanent magnet assisted synchronous reluctance machine," *IEEE Trans. Ind. Appl.*, vol. 54, no. 2, pp. 1349–1359, Mar./Apr. 2018.

[17] B. Wang, J. Wang, A. Griffo, and B. Sen, "Experimental assessments of a triple redundant 9-phase fault tolerant PMA SynRM drive," *IEEE Trans. Ind. Electron.*, vol. 66, no. 1, pp. 772–783, Jan. 2019.

[18] F. Briz, M. W. Degner, A. Zamarron, and J. M. Guerrero, "Online stator winding fault diagnosis in inverter-fed AC machines using high-frequency signal injection," *IEEE Trans. Ind. Appl.*, vol. 39, no. 4, pp. 1109–1117, Jul./Aug. 2003.

[19] K. Kyung-Tae, P. Jun-Kyu, H. Jin, and K. Byeong-Woo, "Comparison of the fault characteristics of IPM-type and SPM-type BLDC motors under inter-turn fault conditions using winding function theory," *IEEE Trans. Ind. Appl.*, vol. 50, no. 2, pp. 986–994, Mar./Apr. 2014.

[20] J. Faiz and I. Tabatabaei, "Extension of winding function theory for nonuniform air gap in electric machinery," *IEEE Trans. Magn.*, vol. 38, no. 6, pp. 3654–3657, Nov. 2002.

[21] B. Wang, J. Wang, A. Griffo, and B. Sen, "A general modeling technique for a triple redundant 3 × 3-phase PMA SynRM," *IEEE Trans. Ind. Electron.*, vol. 65, no. 11, pp. 9068–9078, Nov. 2018.

[22] G. R. Catuogno, G. O. Garcia, and R. Leidhold, "Fault-tolerant inverter for power flow control in variable-speed four-wire permanent-magnet generators," *IEEE Trans. Ind. Electron.*, vol. 62, no. 11, pp. 6727–6736, Nov. 2015.

[23] M. Beltrao de Rossiter Correa, C. B. Jacobina, E. R. Cabral da Silva, and A. M. N. Lima, "An induction motor drive system with improved fault tolerance," *IEEE Trans. Ind. Appl.*, vol. 37, no. 3, pp. 873–879, May/Jun. 2001.

[24] B. Wang, J. Wang, A. Griffo, and B. Sen, "Stator turn fault detection by 2nd harmonic in instantaneous power for a triple redundant fault-tolerant PM drive," *IEEE Trans. Ind. Electron.*, vol. 65, no. 9, pp. 7279–7289, Sep. 2018.

Bo Wang (M'17) received the B.Eng. and M.Sc. degrees in electrical engineering from the Nanjing University of Aeronautics and Astronautics, Nanjing, China, in 2009 and 2012, respectively, and the Ph.D. degree in electronic and electrical engineering from The University of Sheffield, Sheffield, U.K., in 2018.

From 2012 to 2014, he was a Senior Engineer with the Delta Electronics Company Ltd., Nanjing, China. From 2017 to 2018, he was a Research Associate with the Department of Electronic and Electrical Engineering, The University of Sheffield. Since 2018, he has been with the School of Electrical Engineering, Southeast University, Nanjing. His research interests include permanent magnet machine drives, electric traction, and fault tolerant systems.

Jiabin Wang (SM'03) received the B.Eng. and M.Eng. degrees from Jiangsu University, Zhengjiang, China, in 1982 and 1986, respectively, and the Ph.D. degree from the University of East London, London, U.K., in 1996, all in electrical and electronic engineering.

He is currently a Professor in electrical engineering with The University of Sheffield, Sheffield, U.K. From 1986 to 1991, he was with the Department of Electrical Engineering, Jiangsu University, where he served as a Lecturer in 1987 and an Associate Professor in 1990. From 1996 to 1997, he was a Postdoctoral Research Associate with The University of Sheffield and from 1998 to 2001, a Senior Lecturer with the University of East London. His research interests include motion control and electromechanical energy conversion to electric drives for applications in automotive, renewable energy, household appliances, and aerospace sectors.

Dr. Wang is a fellow of the IET.

Antonio Griffo (M'13) received the M.Sc. degree in electronic engineering and the Ph.D. degree in electrical engineering from the University of Napoli "Federico II," Naples, Italy, in 2003 and 2007, respectively.

From 2007 to 2013, he was a Research Associate with The University of Sheffield, Sheffield, U.K., and the University of Bristol, Bristol, U.K. He is currently a Senior Lecturer with the Department of Electronic and Electrical Engineering, The University of Sheffield. His research interests include modeling, control and condition monitoring of electric power systems, power electronics converters, and electrical motor drives, for renewable energy, automotive, and aerospace applications.

Wei Hua (SM'16) was born in Taizhou, China, in 1978. He received the B.Sc. and Ph.D. degrees in electrical engineering from Southeast University, Nanjing, China, in 2001 and 2007, respectively.

From 2004 to 2005, he visited the Department of Electronics and Electrical Engineering, The University of Sheffield, U.K., as a Joint-Supervised Ph.D student. Since 2007, he has been with Southeast University, where he is currently a Professor with the School of Electrical Engineering. He is the author or coauthor of more than 150 technical papers, and he is the holder of 50 patents in his areas of interest. His research interests include the design, analysis, and control of electrical machines.